Similarity of Near-Threshold Energy Dependence of Positronium Formation and Photoionization in Molecules

J. R. Danielson,[1,*] G. F. Gribakin,[2] E. Arthur-Baidoo,[1] and C. M. Surko[1]
[1]Physics Department, University of California San Diego, La Jolla, California 92093, USA
[2]School of Mathematics and Physics, Queen's University Belfast, University Road, Belfast BT7 1NN, United Kingdom

(Received 2 May 2024; revised 10 July 2024; accepted 13 August 2024; published 17 September 2024)

High-resolution measurements of the positronium formation cross sections for positron energies from threshold to 10 eV are presented for aniline ($C_6H_5NH_2$), pyridine (C_5H_5N), and cyclopentane (C_5H_{10}). The data reveal that the measured energy dependence of the cross sections on the excess energy in the near-threshold region (1–2 eV) is nearly identical to that of the corresponding photoionization cross sections. This similarity occurs despite the difference between the basic threshold laws for processes without and with a Coulomb interaction between the final-state particles. It is proposed here that the near-threshold behavior of these two different ionization processes is governed by the vibrational dynamics of the final-state cation. This is supported by comparison of the data with the calculated spectrum of vibronic intensities for the pyridine cation [Trofimov *et al.*, J. Chem. Phys. **153**, 164307 (2020)].

DOI: 10.1103/PhysRevLett.133.123001

Reported here are measurements of the positronium (Ps) formation cross section for a number of polyatomic molecules. Comparison of these cross sections with the corresponding photoionization (PI) cross sections reveals a remarkable similarity in their near-threshold energy dependence. Analysis presented here indicates that this is related to the vibrational spectrum of the molecular cation, and it suggests an unexpected similarity between the underlying leptonic cross sections.

Threshold laws such as the Wigner threshold law [1] have a special place in scattering theory. They predict the energy dependence of a cross section close to a reaction threshold, which depends on the nature of the particles involved (i.e., neutral or charged, with or without a permanent dipole, etc.) [2,3]. This helps one to identify such thresholds and measure the important parameters of nuclear, atomic, and molecular systems, such as the ionization energy, electron affinity, or dissociation energy, by measuring the corresponding cross sections at energies near the threshold (see, e.g., Refs. [4–7]). While much is known about these threshold laws for simple systems, their manifestation for complex systems such as polyatomic molecules, or composite products like Ps, is often quite challenging [8–10].

Positronium, the bound state of a positron and an electron, can be formed in low-energy positron collisions with atoms and molecules. This results in ionization of the target with a threshold $E_{\rm Ps} = E_I - |E_{1s}|$, where E_I is the target ionization energy, and $E_{1s} = -6.803$ eV is the ground-state energy of Ps [11]. This is a charge-exchange reaction in which a molecular electron joins the positron, leaving a cation behind. Positronium formation is the main annihilation channel for galactic positrons [12] and a key process in positron annihilation lifetime spectroscopy of porous materials [13], while its interaction with antiprotons is a means for producing antihydrogen (see [14] and references therein).

Measurements of Ps formation have been made in a wide range of contexts, including studies of atoms and molecules [15–22]. However, beyond a few measurements for noble-gas atoms and H_2, there have been few detailed studies of threshold behavior. Although the behavior at higher energies ($\gtrsim$20 eV above threshold) has been shown to agree with calculations (e.g., [23,24]), there have been virtually no theoretical calculations that predict the cross section near threshold except for the simplest targets [25,26].

Much more is known about photoionization. For many atoms, PI near threshold comes from both direct ionization and autoionization of superexcited (e.g., above-threshold Rydberg) states [27–30]. There is no analog to autoionization transitions in Ps formation, and thus the observed threshold behavior for atoms is quite different [15,20]. A key difference is also that in PI, the attractive Coulomb interaction between the electron and cation results in a steplike onset of the cross section, with $\sigma = \text{const}$ at threshold $E = E_I$; while in Ps formation, the interaction is of short range, with $\sigma \propto \sqrt{E - E_{\rm Ps}}$, according to Wigner's law.

In contrast to atoms, polyatomic molecules have other competing processes. Superexcited states near threshold often lead to neutral dissociation instead of autoionization, and thus the ion signal is dominated by direct ionization [31]. Further, the availability of many vibrational states

*Contact author: jdan@physics.ucsd.edu

means each electronic ionization transition is split into a spectrum of individual vibronic transitions, with intensities given by the respective Franck-Condon factors. As a consequence, when the geometry of the cation is significantly different from that of the neutral, there will be a gap between the adiabatic and vertical transition energies and thus a broadening of the near-threshold onset of the cross section [10]. Until now, such effects have not been considered in studies of ionization by Ps formation.

Presented here are high-resolution measurements of Ps-formation cross sections up to 10 eV, with a focus on the near threshold behavior, for aniline ($C_6H_5NH_2$), pyridine (C_5H_5N), and cyclopentane (C_5H_{10}). These cross sections are compared to near-threshold photoionization mass spectrometry measurements for the same molecules [32,33].

Despite all three molecules being rings, the cross section for each exhibits a distinctly different shape near threshold. However, there are two important features common to all three molecules that are relevant to the comparison. First, near threshold, autoionization is either weak or absent, and so the PI signal is set by direct ionization. Second, the adiabatic and vertical ionization energies for these molecules differ by ∼0.5 eV, and so the cross section onset is broadened by many vibronic transitions. This broadening means that the absolute E_I is often only known to ∼0.1 eV. However, the PI and Ps-formation thresholds are 6.803 eV apart. Hence, if the PI data are downshifted by this amount, then the energy dependences of the cross sections can be compared without any assumptions about the exact ionization energy, eliminating a big source of uncertainty. Lastly, since both measurements are absolute, a comparison of the absolute magnitudes can also be made.

Positronium formation is measured by detecting annihilation, using a room-temperature trap-based positron beam. At positron energies above E_{Ps}, the direct annihilation signal is weak, and thus the annihilation is due to Ps formation. The positron trapping and beam formation process has been described in detail previously [34,35]. Briefly, low-energy positrons from a solid neon moderated ^{22}Na source are magnetically guided into a three-stage buffer-gas trap, where collisions with N_2 and CF_4 molecules lead to trapping and cooling in an electrostatic well. The trapped positrons are carefully pulsed out of the trap into a beam with mean parallel energy ∼1 eV, and a temporal pulse width ∼3 μs [36]. This beam is magnetically guided into the annihilation cell (shown in Fig. 1) where the test gas is introduced [34]. The cell is 26.7 cm long and 4.4 cm in diameter. It has a separately controlled bias potential to set the final interaction energy of the positrons. Baffles in front and back of the cell are used to define the pressure in the cell, which is measured using a capacitance manometer.

Gamma rays from the annihilation are recorded using a single cylindrical CsI(Tl) detector (7 cm in diameter, 6 cm long) located axially at the middle of the cell, with the front face 8.3 cm from the positron beam. The effective field of view along the positron beam is approximately 10 cm FWHM. During a measurement, the electrode at the back of the cell is biased to reflect the beam, so each pulse makes two passes by the detector during a single "bounce." The signal on the detector during the first bounce is integrated to give the total annihilation per pulse of positrons. Positronium is formed in two spin states: 25% is para-Ps ($S = 0$), which decays into two 511 keV γ rays with a lifetime of 125 ps, and 75% is ortho-Ps ($S = 1$), which decays into three γ rays with a lifetime of 140 ns.

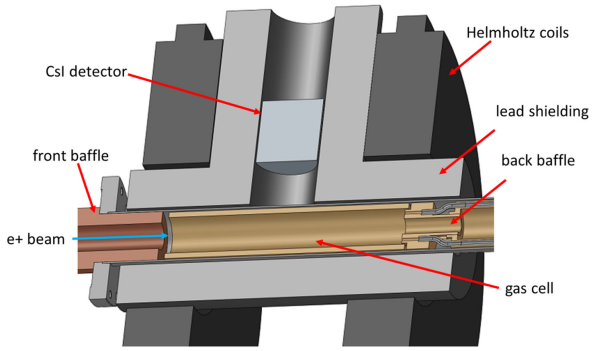

FIG. 1. Cut-away diagram showing the gas cell and γ-ray detector. See text for details.

The assumption is made that the CsI acts as an energy detector [36]. Thus, the signal is proportional to the *total* energy of the γ rays, which is 1022 keV for both para- and ortho-Ps. Thus, averaged over many decays (which are unoriented in space), the energy per steradian, and hence the detection efficiency, is the same for both states. At very low Ps energies (e.g., ≤ 0.03 eV), 90% of the ortho-Ps will decay before hitting the surrounding electrode. At higher energies, they will hit the walls and decay via two γ rays [37], likely after multiple bounces.

One caveat is that, if the differential Ps-formation cross section (unknown for these molecules) were strongly forward peaked, ortho-Ps with energies ≥ 1 eV formed at the entrance to the cell could pass by the detector before annihilating or hitting the cell electrode (i.e., a loss cone with half-angle ∼0.16 rad). Tests changing the detector field of view indicate this is not the case. Further, as shown in Fig. 2(a), measurements for pyridine using a different technique [38] agree with the data presented here. Thus, such loss-cone effects do not appear to affect the detector efficiency.

The Ps-formation cross sections for the three molecules are shown in Fig. 2(a) for energies from threshold up to 10 eV. The vertical lines are the estimated Ps thresholds $E_{\mathrm{Ps}} = E_I - 6.803$ eV, using $E_I = 7.72$ eV for aniline [39], $E_I = 9.199$ eV for pyridine [40], and $E_I = 10.33$ eV for cyclopentane [39]. For comparison, the measured Ps cross section from Ref. [38] is shown as solid black circles. The

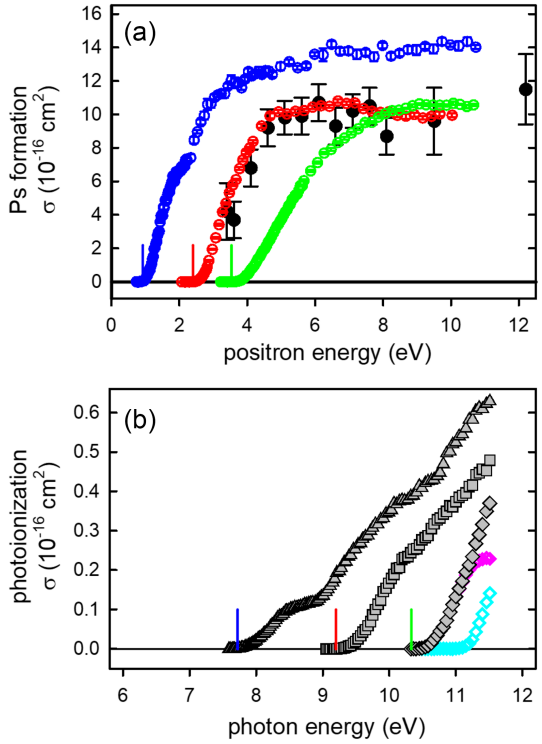

FIG. 2. (a) Measured Ps-formation cross section for aniline (blue circle), pyridine (red circle), cyclopentane (green circle). Error bars are statistical and comparable to the size of the symbols in most cases. Black dots with error bars show the cross section for pyridine from Ref [38] measured using a different technique. (b) Measured PI cross section for aniline (parent, gray triangle) [32], pyridine (parent, gray square) [32], cyclopentane (total, gray diamond; parent, magenta diamond; sum of other masses, cyan diamond) [33]. In panel (a), the vertical lines mark the approximate Ps thresholds, $E_{\mathrm{Ps}} = E_I - 6.803$ eV, and in panel (b) the vertical lines mark the approximate ionization energies E_I; aniline (blue), pyridine (red), and cyclopentane (green).

present cross section for pyridine matches the previous data in both shape and magnitude but with significantly higher resolution.

All three molecules show a relatively rapid rise near threshold before reaching a plateau 3–4 eV above threshold. Aniline and pyridine show some evidence of structure in the signal during the rising portion. Aniline displays a mild step before a second rise, and pyridine shows a slight change in slope after ~1 eV. Cyclopentane shows a steady rise with no visible structure.

The absolute PI measurements from Refs. [32,33] are shown in Fig. 2(b). The photon energy varied from threshold up to 11.5 eV, with a resolution of $E/\Delta E \sim 500$, which gives $\Delta E \sim 20$ meV for $E \sim 10$ eV [32]. The solid lines indicate the respective E_I values [39,40]. For aniline and pyridine, only the parent ion was observed. For cyclopentane, fragmentation begins near ~11 eV. As with the Ps-formation data, aniline and pyridine show evidence of structure in the signal, whereas the total ion count for cyclopentane only shows a steady rise. The absolute cross sections for PI are smaller than Ps by an order of magnitude.

To compare the PI and Ps cross sections, the energies of the PI data are reduced by 6.803 eV. Then a single multiplicative factor is used to bring the magnitude of the PI data near threshold into best fit. For aniline, pyridine, and cyclopentane, the factors are 57, 22.5, and 7.5, respectively. The scaled PI data and the Ps measurements are shown in Fig. 3. For each molecule, the data overlap is excellent over the first 1–2 eV above threshold. Panel (b) also shows the energy spreads of the positron and photon beams (FWHM of ~35 and ~25 meV [32], respectively). In both cases the energy spread is comparable to the data-point spacing and small compared to features in the cross sections.

For aniline, the agreement between the PI and Ps-formation data includes the rise to the first step around 1.5 eV from threshold. Above this, the scaled PI data rises more rapidly than the Ps data until arriving at a second step about 2.5 eV from threshold [see Fig. 2(b)]. Above this energy, the Ps cross section increases slowly over the next 4–5 eV. In contrast, the PI curve in Fig. 2(b) has a third distinct rise above this energy. From the photoelectron spectra (PES) [41], the energies of the two highest occupied electron orbitals are well separated, and correlate with the first and second rises in the PI signal. Thus, the structure in the first 2 eV above threshold can be associated with these orbitals. Looking at the magnitudes of the cross sections, the relative contribution of HOMO − 1 to the PI cross section appears to be a factor of 2 larger than its contribution to Ps formation. This seems to be a general trend, where the contributions of deeper-lying electron orbitals to the Ps-formation cross section becomes progressively smaller compared to their contributions to PI.

For pyridine, Fig. 2(b), the overlap is very good over 2 eV above threshold. This includes the change in slope at ~1 eV above threshold. At excess energies above 2 eV, the Ps signal begins to flatten out, while the PI signal continues to increase. Other (nonabsolute) PI measurements have also observed a steady rise in the signal above this energy [42,43].

From the PES [42,44] and more recent high-resolution, threshold photoelectron spectra measurements [40], it is seen that there are two electron orbitals ($7a_1$ and $1a_2$) whose vibrationally broadened contributions overlap strongly within ~0.5 eV of the threshold. The third orbital ($2b_1$) is well separated, with ionization energy ~1 eV higher, which correlates with the change in slope in the data. The agreement between the Ps-formation and PI data suggests that, in contrast to aniline, the relative contributions of the three highest occupied molecular orbitals to the two processes are similar.

For cyclopentane [Fig. 3(c)], the PI cross section is available only within 1.2 eV of the threshold. Over this limited range, the overlap of the Ps and PI data is excellent. As with pyridine, in cycloalkanes several orbitals are

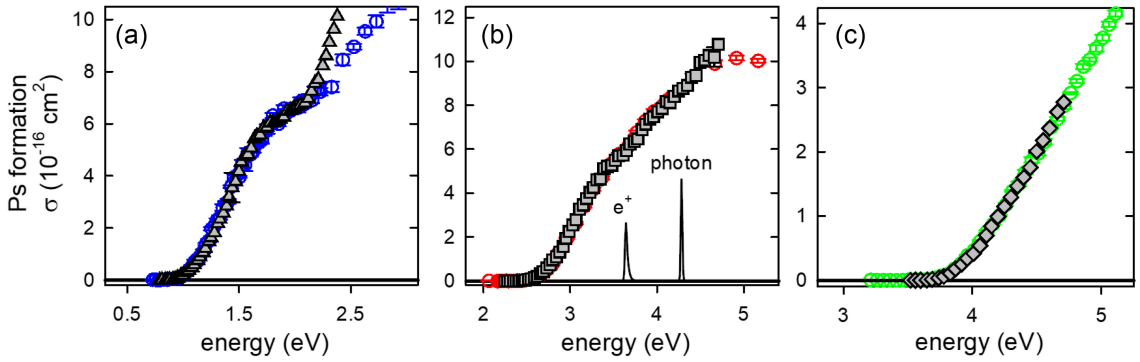

FIG. 3. Comparison of Ps and PI data: (a) aniline, (b) pyridine, (c) cyclopentane, same symbols as Fig. 2. The energy scale of each PI curve was downshifted by 6.803 eV, and the magnitude was multiplied by a scale factor to match the Ps data near threshold. Panel (b) includes examples of the positron and photon beam distributions (solid black lines). See text for details.

accessible within ~1 eV above threshold [45,46]. The close overlap of the Ps and PI data again implies that the relative contributions of these orbitals to the two cross sections are about the same. The PI data shows the onset of fragmentation within 1 eV of threshold. This is shown by the magenta (parent ion) and cyan (other mass fragments) data in Fig. 2(b). The comparison in Fig. 3(c) is with the *total* PI (solid diamonds), so the fragmentation does not appear to make a difference for the PI and Ps comparison. This is consistent with the fact that fragmentation of the cyclopentane ion is slow compared to the electron removal in either PI or Ps formation.

Figure 3 shows that the rise of the cross sections near threshold does not follow the basic threshold laws for the leptonic cross sections for photoionization ($\sigma = \text{const}$ at threshold) or Ps formation ($\sigma \propto \sqrt{E - E_{\text{Ps}}}$). Instead, the behavior of both cross sections is nearly identical but molecule-specific. This suggests that it is determined by the vibrational spectrum of the molecular cation and corresponding Franck-Condon factors, or more generally, the vibronic intensities. The latter describes the probability of excitation of final vibronic states of the cation that result from mixing of vibrational excitations of closely spaced electronic states (such as those obtained by the removal of $7a_1$ and $1a_2$ electrons in pyridine [47]).

A significant difference between the vertical and adiabatic ionization energies (0.33 eV in aniline, 0.46 eV in pyridine, and 0.68 eV in cyclopentane) means that many vibrational states are excited in the process of ionization. Using the known vibrational frequencies of these molecules, one estimates that with only 0.5 eV excess energy, the number of such states ranges from 10^4 (pyridine, the smallest of the three molecules) to 10^6 (cyclopentane, the largest). These numbers rise to 10^7–10^{10} by 1 eV. When this energy range includes several electron orbitals, calculation of the vibronic intensities becomes challenging. The corresponding spectrum of vibronic excitations forms a quasicontinuum, which can be seen in the PES data for these molecules [40,41,45].

Recently, Trofimov and collaborators published calculations of the vibronic spectra of A_1, A_2, and B_1 symmetries, which originate from the ionization of the highest occupied orbitals ($7a_1$, $1a_2$, and $2b_1$) of pyridine [47]. Except for a small shift in energy (~0.13 eV), the calculated spectra that use equal weights for the three symmetries agree well with recent high-resolution He-I PES data [48]. Thus, we use the calculated intensities to analyze the cross sections for pyridine.

Assuming a steplike onset of the cross sections, we model the signal as $\sigma(E) = \sum_{\alpha,i} C_\alpha I_{\alpha i} \Theta(E - E_{\alpha i})$, where the sum is over the cation vibronic state symmetries α and states i of each symmetry, $I_{\alpha i}$ and $E_{\alpha i}$ are the intensities and energies calculated in Ref. [47], and $\Theta(x)$ is a step function [$\Theta(x) = 0$ for $x < 0$, $\Theta(x) = 1$ for $x \geq 0$]. The calculation includes 2267 A_1, 2456 A_2, and 2795 B_2 states, which span a 2 eV energy range near threshold.

Two models are constructed. In Model 1, all energies are increased by 0.13 eV and we use equal weights C_α, chosen to fit the cross section near threshold (dashed line in Fig. 4).

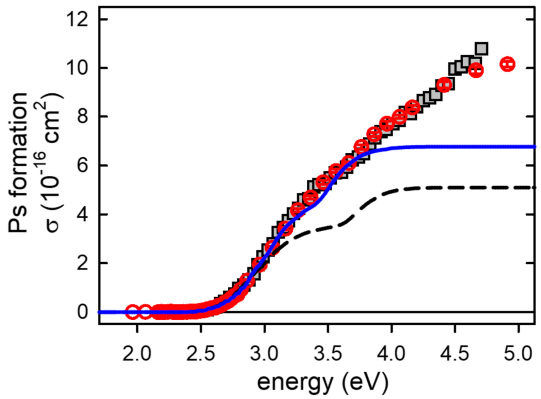

FIG. 4. Pyridine Ps-formation (red circle) and shifted and scaled photoionization (black solid square) data from Fig. 3(b) are compared to a model using the calculated vibronic intensities from Ref. [47]. Model 1 (black dashed line); Model 2 (blue solid line). See text for details.

In Model 2, the energies and weights are adjusted separately. The energies of the A_1, A_2, and B_1 states are shifted by 0.13, 0.18, and −0.07 eV, respectively, and the weights are in the ratio 1:1.8:1.6. This sum is scaled to match the data at threshold (solid blue line in Fig. 4). The energy shifts account for uncertainties in the orbital energies and the weights allow for different leptonic cross section magnitudes.

Both models show good agreement with the data between threshold (2.4 eV) and 3 eV. At higher energies, the change in slope at ∼3.5 eV is correlated with the onset of the contribution of B_1 symmetry states that are mostly due to the removal of the $2b_1$ electron. Model 2 shows good agreement with the data up to ∼1.5 eV above threshold. Thus, in the energy range of the first three orbitals, the sum of the vibronic intensities appears to explain the shape of the energy dependence. Additionally, the calculations of Ref. [47] assumed that the molecule is in the ground vibrational state, while the experiments were done at 295 K, so temperature effects may need to be considered for a more accurate comparison between theory and experiment.

As seen in Fig. 4, beyond the third orbital, both the Ps and PI data continue to increase. From the PES data, there is a gap of almost 2 eV between the $2b_1$ and the next orbital [40,44]. Hence, the rise is not likely due to the next orbital, and its origins are unclear.

In summary, presented here are high-resolution measurements of the near-threshold Ps-formation cross sections for aniline, pyridine, and cyclopentane. A comparison of these data with the PI cross sections shows that they have the same dependence on the excess energy when scaled to the same magnitude. This energy dependence is attributed to the accumulated intensity of vibronic transitions to the final cation states, which form a quasicontinuum. For pyridine, this has been verified using the calculated vibronic transitions associated with ionization of the three highest occupied electron orbitals. The observed agreement implies that, for both PI and Ps formation, the leptonic cross sections are either constant or very weak functions of excess energy.

Our observations also indicate that Ps formation in these molecules is a direct process not mediated by formation of a positron-molecule complex. This is in contrast to electron-molecule collisions that are often dominated by the presence of resonances [3,49].

For molecules that do not have extensive vibronic transitions, or have significant PI resonances near threshold, this similarity may break down and could be tested by future experiments. It is hoped that these results will also stimulate further theoretical work, particularly the leptonic cross sections for PI and Ps formation for these molecules.

Acknowledgments—We are grateful to A. B. Trofimov for providing their results in numerical form, and for useful discussions. We thank V. Averbukh and S. Patchkovskii for useful discussions. We also thank D. R. Witteman and D. Morschl-Villa for technical assistance, and S. Ghosh for useful discussions. The work was supported by the UCSD Foundation and U.S. NSF Grant PHY-2306404.

[1] E. P. Wigner, Phys. Rev. **73**, 1002 (1948).
[2] H. R. Sadeghpour, J. L. Bohn, M. J. Cavagnero, B. D. Esry, I. I. Fabrikant, J. H. Macek, and A. R. P. Rau, J. Phys. B **33**, R93 (2000).
[3] H. Hotop, M.-W. Ruf, M. Allan, and I. I. Fabrikant, Adv. At. Mol. Opt. Phys. **49**, 85 (2003).
[4] D. Leimbach, J. Karls, Y. Guo *et al.*, Nat. Commun. **11**, 3824 (2020).
[5] K. Michishio, S. Kuma, Y. Nagata, L. Chiari, T. Iizuka, R. Mikami, T. Azuma, and Y. Nagashima, Phys. Rev. Lett. **125**, 063001 (2020).
[6] M. Simpson, M. Nötzold, T. Michaelsen, R. Wild, F. A. Gianturco, and R. Wester, Phys. Rev. Lett. **127**, 043001 (2021).
[7] J. E. Navarro Navarrete, M. Nichols, A. Ringvall-Moberg, J. Welander, D. Lu, D. Leimbach, M. K. Kristiansson, G. Eklund, M. Raveesh, R. Chulkov, V. Zhaunerchyk, and D. Hanstorp, Phys. Rev. A **109**, 022812 (2024).
[8] I. I. Fabrikant, A. W. Bray, A. S. Kadyrov, and I. Bray, Phys. Rev. A **94**, 012701 (2016).
[9] S. J. Ward and J. H. Macek, Phys. Rev. A **62**, 052715 (2000).
[10] P. M. Guyon and J. Berkowitz, J. Chem. Phys. **54**, 1814 (1971).
[11] M. Charlton and J. W. Humberston, *Positron Physics* (Cambridge University Press, Cambridge, England, 2001), Vol. 11.
[12] E. Churazov, S. Sazonov, S. Tsygankov, R. Sunyaev, and D. Varshalovich, Mon. Not. R. Astron. Soc. **411**, 1727 (2011).
[13] D. W. Gidley, H.-G. Peng, and R. S. Vallery, Annu. Rev. Mater. Res. **36**, 49 (2006).
[14] C. M. Rawlins, A. S. Kadyrov, A. T. Stelbovics, I. Bray, and M. Charlton, Phys. Rev. A **93**, 012709 (2016).
[15] K. Ratnavelu, M. J. Brunger, and S. J. Buckman, J. Phys. Chem. Ref. Data **48**, 023102 (2019).
[16] M. J. Brunger, S. Buckman, and K. Ratnavelu, J. Phys. Chem. Ref. Data **46**, 023102 (2017).
[17] J. Machacek, F. Blanco, G. Garcia, S. Buckman, and J. Sullivan, J. Phys. B **49**, 064003 (2016).
[18] J. R. Machacek, C. Makochekanwa, A. C. Jones, P. Caradonna, D. S. Slaughter, R. P. McEachran, J. P. Sullivan, S. J. Buckman, S. Bellm, B. Lohmann *et al.*, New J. Phys. **13**, 125004 (2011).
[19] M. Thornton and P. G. Coleman, J. Phys. B **44**, 145201 (2011).
[20] L. Chiari and A. Zecca, Eur. Phys. J. D **68**, 1 (2014).
[21] J. Archer, S. Trilov, and P. Coleman, J. Phys. Conf. Ser. **443**, 012001 (2013).
[22] P. G. Coleman, N. J. Culver, and B. M. W. M. Dowler, Phys. Rev. A **87**, 012712 (2013).
[23] L. Dunlop and G. Gribakin, Nucl. Instrum. Methods Phys. Res., Sect. B **247**, 61 (2006).

[24] R. McEachran and A. Stauffer, J. Phys. B **46**, 075203 (2013).
[25] J. Humberston, P. Van Reeth, M. S. T. Watts, and W. E. Meyerhof, J. Phys. B **30**, 2477 (1997).
[26] P. V. Reeth and J. W. Humberston, J. Phys. B **32**, 3651 (1999).
[27] J. Morrison, H. Hurzeler, M. G. Inghram, and H. Stanton, J. Chem. Phys. **33**, 821 (1960).
[28] J. Morrison, J. Chem. Phys. **40**, 2488 (1964).
[29] J. Berkowitz, H. Ehrhardt, and T. Tekaat, Z. Phys. **200**, 69 (1967).
[30] C. Batten, J. A. Taylor, and G. Meisels, J. Chem. Phys. **65**, 3316 (1976).
[31] H. Koizumi, J. Chem. Phys. **95**, 5846 (1991).
[32] M. Xie, Z. Zhou, Z. Wang, D. Chen, and F. Qi, Int. J. Mass Spectrom. **303**, 137 (2011).
[33] Z. Zhou, L. Zhang, M. Xie, Z. Wang, D. Chen, and F. Qi, Rapid Commun. Mass Spectrom. **24**, 1335 (2010).
[34] L. D. Barnes, S. J. Gilbert, and C. M. Surko, Phys. Rev. A **67**, 032706 (2003).
[35] M. Natisin, J. Danielson, and C. Surko, Phys. Plasmas **22**, 033501 (2015).
[36] J. R. Danielson, S. Ghosh, E. Arthur-Baidoo, D. R. Witteman, and C. M. Surko, Phys. Rev. A **108**, 032801 (2023).
[37] D. W. Gidley, D. McKinsey, and P. W. Zitzewitz, J. Appl. Phys. **78**, 1406 (1995).
[38] D. Stevens, T. Babij, J. Machacek, S. Buckman, M. J. Brunger, R. White, G. García, F. Blanco, L. Ellis-Gibbings, and J. Sullivan, J. Chem. Phys. **148**, 144308 (2018).
[39] S. G. Lias, *NIST Chemistry Webbook, NIST Standard Reference Database*, 69th ed., edited by P. J. Linstrom and W. G. Mallard (National Institute of Standards and Technology, Gaithersburg MD, 20899, 2024), Chap. Ionization Energy Evaluation.
[40] M. A. Śmiałek, M. A. MacDonald, S. Ptasińska, L. Zuin, and N. J. Mason, Eur. Phys. J. D **70**, 1 (2016).
[41] T. Debies and J. Rabalais, J. Electron Spectrosc. Relat. Phenom. **1**, 355 (1972).
[42] C. Goffart, J. Momigny, and P. Natalis, Int. J. Mass Spectrom. Ion Phys. **3**, 371 (1969).
[43] G. Vall-llosera, M. Coreno, P. Erman, M. A. Huels, K. Jakubowska, A. Kivimäki, E. Rachlew, and M. Stankiewicz, Int. J. Mass Spectrom. **275**, 55 (2008).
[44] I. Reineck, R. Maripuu, H. Veenhuizen, L. Karlsson, K. Siegbahn, M. Powar, W. N. Zu, J. M. Rong, and S. Al-Shamma, J. Electron Spectrosc. Relat. Phenom. **27**, 15 (1982).
[45] A. W. Potts and D. G. Streets, J. Chem. Soc., Faraday Trans. 2 **70**, 875 (1974).
[46] G. Bieri, F. Burger, E. Heilbronner, and J. P. Maier, Helv. Chim. Acta **60**, 2213 (1977).
[47] A. Trofimov, A. Skitnevskaya, E. Grigoricheva, E. Gromov, and H. Köppel, J. Chem. Phys. **153**, 164307 (2020).
[48] S.-Y. Liu, K. Alnama, J. Matsumoto, K. Nishizawa, H. Kohguchi, Y.-P. Lee, and T. Suzuki, J. Phys. Chem. A **115**, 2953 (2011).
[49] I. Bald, J. Langer, P. Tegeder, and O. Ingólfsson, Int. J. Mass Spectrom. **277**, 4 (2008).